arXiv:2607.18779v1 [cs.CV] 21 Jul 2026

CGMap: A Geospatially Aware Deep Learning Framework for Crop Gap Mapping Using UAV

Karan Sharma[0009−0004−5371−7280], Rajiv Ranjan[0009−0008−3248−7374], Dinesh Kumar[0009−0000−4952−0742], and Shashank Tamaskar[0000−0002−9497−2817]

Robotics and Autonomous Systems, Plaksha University, Mohali, India
karan.sharma@plaksha.edu.in, rajiv.ranjan@plaksha.edu.in, dinesh.kumar1@plaksha.edu.in, shashank.tamaskar@plaksha.edu.in

Abstract. In India, crop germination is primarily monitored by visual inspection and manual counting, which are prone to errors, despite their crucial role in determining eventual yield potential. This paper highlights a deep learning based pipeline which uses object detection methods and drone imagery to assess and provide a precise count of sugarcane germination in fields. The approch uses a pre-trained AI model to find germinated plant sampling and identify gaps, also known as "bald spots", which restricts field productivity. The techniques used here relies on the YOLOV8 architecture, which was trained on a carefully selected dataset of UAV photos taken in various agroclimatic zones of India. Here, we bring upon a novel orientation-normalization technique that uses minimum Spanning Trees (MST) to account for variations in planting geometry, allowing for dependable row and column extraction across a variety of field layouts. By converting detected seedlings into spatial point clouds, emergence gaps can be inferred from the anticipated spacing between plants. A geospatial germination map exported in Well-Known Text (WKT) format is the end result, and it can be easily incorporated into GIS platforms used by sugar mills and agronomists to direct transplant initiatives. Timely interventions based on the insights provided by the algorithm can significantly increase yield, resulting in higher profits. Hence, support proper allocation of resources, avoid wastage, and enhance long-term sustainability.

Keywords: Crop germination monitoring · Deep learning pipeline · Sugarcane germination · Object detection · Bald spots detection · Emergence gap detection. · Pattern Recognition

1 Introduction

Remote sensing has emerged as a transformative tool in modern agriculture, enabling large-scale, continuous, and non-destructive crop monitoring [1,2]. The crop of interest in this paper, Sugarcane (*Saccharum officinarum*) [3] is a critical crop of the global agricultural economy, serving as the main source of sugar, ethanol and related by-products. India, among other producing nations, is the second largest sugarcane grower in the world, accounting for more than 5000

metric tons (LMT), following Brazil[4,5].India has now grown to be the worlds largest sugar producer and the second largest exporter, providing the livelihoods of over 50 million farmers and with almost 10% of the rural population in its cultivation, processing and supply chain [6].

Despite its scale and strategic importance, sugarcane production in India faces persistent challenges in achieving a uniform cropping pattern, especially during the early germination phase [7,8,9]. Uniform germination is a key determinant of eventual and final yield, as localized zones of missing or failed germination, colloquially known as "bald spots" or "skips" can lead to unevenness of density, suboptimal resource utilization, and significant yield losses. Bald spots can be attributed to a complex interplay of environmental, mechanical, and biological factors making it necessary to detect them early and find measures to eliminate them

Collectively, these factors underscore the importance of timely detection and spatial diagnosis of bald spots to enable corrective actions, such as transplantation, spot fertilization, or pest control strategies that are critical for maximizing crop stand and overall field productivity. if not identified and replanted early will contribute to yield reductions of upto 10–15 tonnes per hectare, a figure corroborated by field reports from farmers who estimate 20–30% productivity losses due to undetected bald patches during the critical early weeks of growth [10,11,12,5].

Traditionally, the germination of sugarcane saplings assessment and bald spot identification is carried out by manual field inspections that are labor intensive, time-consuming, and infeasible on a large scale.The emergence of precision agriculture, particularly with umanned aerial vehicles (UAVs) and drone based imaging has provided a great alternative [13,14]. UAVs equipped with high-resolution cameras help rapidly collect data in large areas in single flights, enabling near-real-time crop monitoring. The main challange lies in converting raw high resolution imagery into agronomic insights, these might require techniques likes computer vision and spatial analysis [15].

This study highlights a scalable, automated and adaptive pipeline leveraging YOLOv8 [16] for sugarcane detection, OpenCV [17] for row and column detection and Rasterio [18] for spatial analysis. This help us detect individual sugarcane seedlings from drone imagery and find bald spots with precision. A novel orientation correction method using MSTs [19] is also implemented to standardize field geometry and extract meaningful row-column structure data even in irregular or an off-axis farms. The germination maps are then exported in Geographical Information System (GIS)-compatible formats, providing a quick and reliable integration with farm management systems and decision-making tools for agronomy.

By automating this bald spot detection during the early growth window, this pipeline empowers the farm managers and the sugar mills to take timely transplantation on the farms, improving field uniformity and yield potential substantially. While this study is focused on sugarcane in North India, the pipeline is

also transferable to other row crops this contributes to the broader adoption of data-driven and sustainable agriculture.

2 Materials and Methods

2.1 Study Area, UAV Platform and Image Acquisition

Our study focuses on Sugarcane fields in Asmoli, Uttar Pradesh, India, located between 23°52'–30°28' N latitudes and 77°05'–84°38' E longitudes in fertile alluvial plains of the Indo-Gangetic floodplain of north central India, with elevations ranging from approximately 200 to 300m above sea level. The region's soils are predominantly sandy loam to clay loam, known for their high agricultural potential, although they feature localized sandy and loess deposits [20]. While generally fertile, parts of the area face salinity and alkalinity issues, primarily due to over-irrigation [21]. Despite these climatic and edaphic challenges, the combination of deep alluvial soils, effective irrigation infrastructure, and ample monsoonal rainfall supports the intensive cultivation of sugarcane, wheat, and rice. Sugarcane, in particular, thrives under these conditions. However, uniform crop emergence continues to be hindered by inconsistencies in summer sowing conditions, underscoring the need for timely agronomic interventions.

Phantom 4 Multispectral drone, developed by DJI was used to capture the UAV imagery for this study. As highlighted and optimized in previous literature, image acquisition for this study was conducted at flight altitudes of 37.8 and 75.6 meters [22], which yielded a ground sampling distance (GSD) of approximately 2 cm/pixel and 4 cm/pixel. In order to ensure sufficient coverage and photogrammetric accuracy, a front overlap of 80% and a side overlap of 75% were maintained during all flights.

2.2 Orthomosaic Generation and Image Preprocessing

Pix4D Fields , a commercial photogrammetry software was used to process the raw aerial images acquired from UAV flights and to generate high-resolution, orthorectified mosaics (orthomosaics) for each surveyed field. Spatial geometry and radiometric fidelity were preserved in these orthomosaics for providing georeferenced 2D maps suitable for pixel-accurate object detection.

To prepare the data for model training and inference, the following preprocessing steps were applied:

Each orthomosaic was divided into smaller image tiles of size 300×300 pixels using a sliding window approach with 10% overlap to preserve boundary information. Tiles with poor visibility due to shadows, flooding, or motion blur were manually filtered out. Finally, all selected tiles were converted to standard RGB format and resized to 640×640 pixels to match YOLOv8 input dimensions.

The resulting image set formed the input dataset for object detection and annotation.

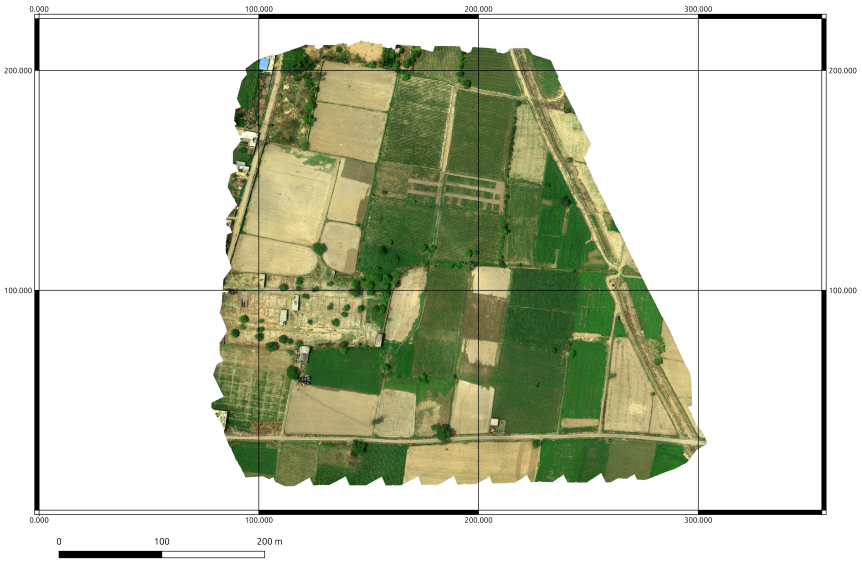


Fig. 1: Georeferenced stitched orthomosaic obtained from UAV.

2.3 Manual Annotation and YOLOv8 Model Training

Approximately 600 image tiles were annotated manually using the open-source web tool `Makesense.AI`. Each visible sugarcane sapling was bounded with a rectangular box and labeled as class `plant`. The annotations were exported in YOLO format, containing:

- Class ID (e.g., `0` for plant)
- Normalized bounding box center coordinates (x, y)
- Normalized width and height (w, h)

The annotated dataset was randomly partitioned into:

- 80% training set
- 20% validation set

For the detection of small, densely spaced plant instances under variable lighting and background conditions, A model was required that combined detection accuracy, computational efficiency, and ease of deployment, YOLOv8 strikes all the requirements and proved to be particularly suited for field-scale agricultural analysis. Unlike two-stage detectors such as Faster R-CNN or lightweight CNN classifiers that lack spatial localization, YOLOv8 provides a single-stage, real-time detection framework with robust feature extraction and anchor-free.

The detection model was implemented using YOLOv8n, a variant from the YOLOv8 family [23]. YOLOv8 introduces key improvements over previous versions, including:

- An anchor-free detection head for better generalization and simplicity.
- A decoupled head for classification and regression tasks.
- Enhanced training stability and performance through modern backbone modules (C2f, SPPF).

Training was conducted using the Ultralytics YOLOv8 framework, with the following hyperparameters:

- Initial learning rate: 0.01
- Batch size: 16
- Epochs: 150
- Optimizer: Stochastic Gradient Descent (SGD) with momentum
- Loss function: Complete IoU (CIoU) loss for bounding box regression

Data augmentation was applied during training (horizontal flipping, scaling, mosaic), and model convergence was monitored using validation mean Average Precision (mAP). Post-training evaluation indicated reasonable detection performance, suitable for field-scale deployment. The detailed experimental results and visualizations are provided in Appendix A.

2.4 Detection, Centroid Extraction, and Point Cloud Generation

A sliding window inference strategy was used to apply the trained YOLOv8m model to the full-resolution orthomosaics. Each detected bounding box was post-processed to compute its centroid:

$$c_i = \left(x_i + \frac{w_i}{2},\ y_i + \frac{h_i}{2} \right)$$

where (x_i, y_i) and (w_i, h_i) are the top-left corner and dimensions of the bounding box, respectively.

A 2D point cloud was generated by projecting these centroids back into the global coordinate system (via georeferencing metadata):

$$\mathcal{P} = \{c_1, c_2, \ldots, c_n\}, \quad c_i \in \mathbb{R}^2$$

Spacial mosaics were cropped through the reference of boundary polygons provided in Well-Known Text (WKT) format by the sugar mill, isolating individual farms. A 5-meter buffer was reinforced around each polygon for ensuring complete inclusion of edge rows, and prevention of detection losses due to spatial clipping.

The subsequent sections discuss the resulting point cloud datasets formed the basis for spatial analysis, including MST-based row extraction and bald spot detection.

2.5 Spatial Normalization via Minimum Spanning Tree

Let the set of detected plant centroids be:

$$\mathcal{P} = \{p_1, p_2, \ldots, p_n\}, \quad p_i \in \mathbb{R}^2 \tag{1}$$

where $p_i = [x_i, y_i]^T$ denotes the 2D coordinates of the ith plant.

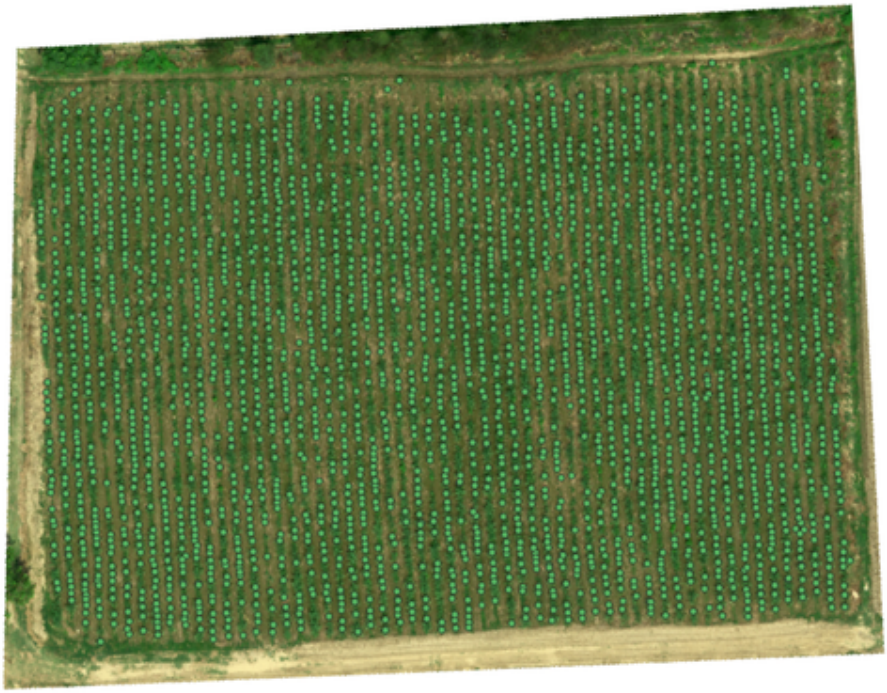


Fig. 2: Image overlaid with AI detection for sugarcane plant centroids, marked with green dots.

Construct a fully connected undirected graph $G = (\mathcal{P}, E)$, where each edge $e_{ij} \in E$ connects nodes p_i and p_j, and has a Euclidean distance weight:

$$w_{ij} = \|p_i - p_j\|_2 \tag{2}$$

Compute a Minimum Spanning Tree (MST) using a standard algorithm such as Prim's [24] or Kruskal's [25], denoted:

$$T = (\mathcal{P}, E_T) \subseteq G \tag{3}$$

such that:

$$\sum_{e_{ij} \in E_T} w_{ij} \quad \text{is minimized.} \tag{4}$$

To isolate intra-row connections (connections along the same planting row), apply a distance threshold:

$$w_{ij} < \theta, \quad \text{where } \theta = d_1 - \alpha_1 \tag{5}$$

where:

- d_1 is the typical distance between adjacent rows (inter-row spacing),
- α_1 is a tolerance margin accounting for natural variability or measurement noise.

This filtering produces disconnected subgraphs $T_1, T_2, \ldots, T_k \subseteq T$, each corresponding to an individual planting row.

For each subgraph T_k, define the unit direction vectors along edges:

$$\boldsymbol{u}_{ij} = \frac{p_j - p_i}{\|p_j - p_i\|_2}, \quad \forall e_{ij} \in T_k \tag{6}$$

The average row orientation vector is then:

$$\boldsymbol{v} = \frac{1}{|E_{T_k}|} \sum_{e_{ij} \in E_{T_k}} \boldsymbol{u}_{ij} \tag{7}$$

The alignment angle with respect to the vertical axis is computed as:

$$\theta^* = \arccos\left(\frac{\boldsymbol{v} \cdot \boldsymbol{y}}{\|\boldsymbol{v}\|}\right), \quad \boldsymbol{y} = \begin{bmatrix} 0 \\ 1 \end{bmatrix} \tag{8}$$

where $\boldsymbol{y}$ is the unit vector along the North–South direction.

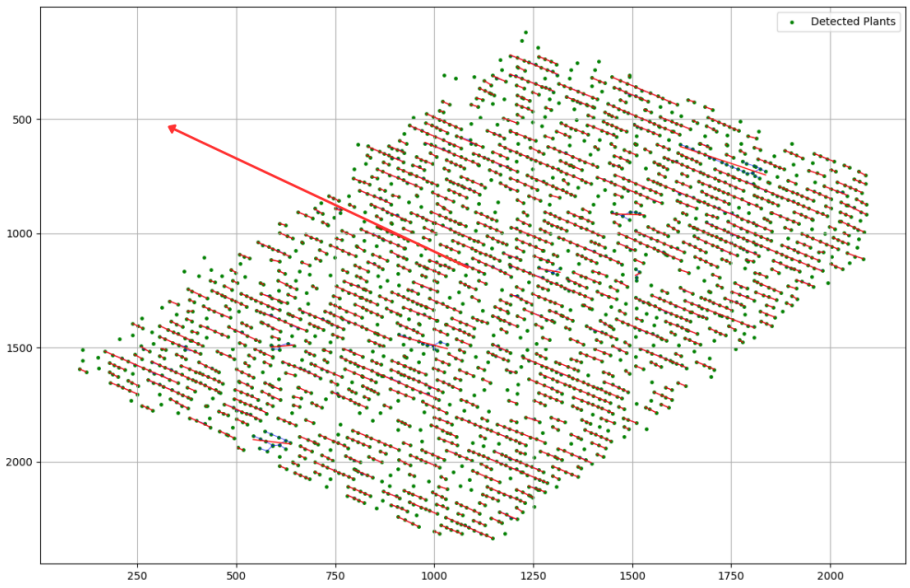


Fig. 3: Point cloud marked with unit vector $\boldsymbol{y}$ along the North–South direction.

Finally, all points p_i are rotated by θ^* (Eq. 8) to yield a North–South aligned point cloud $\mathcal{P}'$.

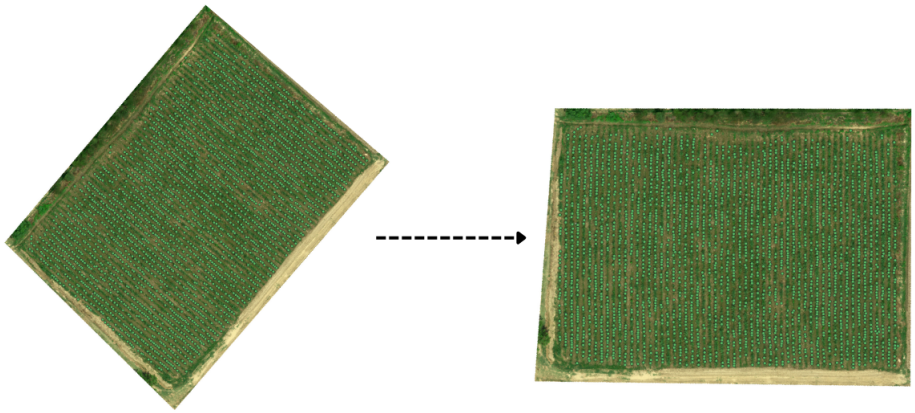
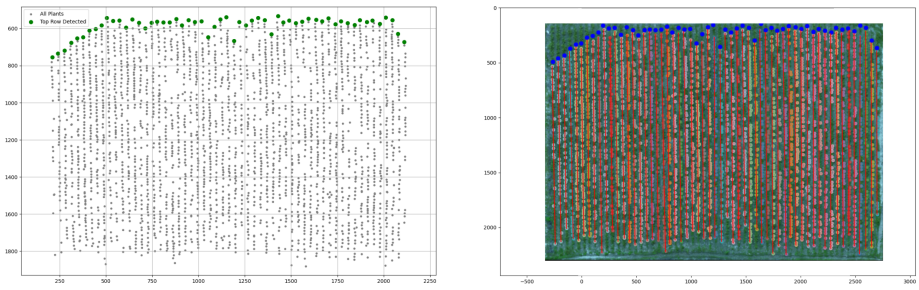


Fig. 4: Spatially normalized image, $\theta^* = 127.6°$.

2.6 Row and Column Extraction and Gap Detection

After alignment, perform column detection on the rotated set $\mathcal{P}'$ by applying a sweeping vertical-line algorithm to identify candidate column lines from the top-most and bottom-most points in each slice.



(a) Sugarcane point cloud marked with topmost points for each slice.

(b) Column identification from sugarcane plant points using line fitting.

Fig. 5: (a) Line sweep for topmost points and (b) fitted lines for column identification in sugarcane plant point cloud.

Each crop column is identified by first fitting a best-fit line to the plant points in that column using linear regression:

$$\hat{y} = mx + b \tag{9}$$

A plant point is assigned to a column if its perpendicular distance to the fitted line is less than $\frac{s_c}{2}$, where s_c is the expected column spacing.

For each column, the plant points are projected onto the fitted line, and the inter-plant distances are computed as:

$$d_i = \|p'_{i+1} - p'_i\|_2 \tag{10}$$

Gaps are identified where:

$$d_i > d_2 + \alpha_2 \tag{11}$$

where d_2 is the expected plant-to-plant spacing and α_2 is a tolerance margin.

Each detected gap is stored as a geometric entity $g_j \in \mathcal{G}$, forming the set:

$$\mathcal{G} = \{g_1, g_2, \ldots, g_m\} \tag{12}$$

The final spatial outputs consist of:

- $\mathcal{P}'$: detected plant centroids (North–South aligned),
- $\mathcal{L}$: column lines,

– $\mathcal{G}$: inferred gaps.

All spatial layers are exported in `WKT` format for GIS visualization and downstream agronomic analysis.



Fig. 6: `WKT` file plotted on QGIS with the original orthomosaic as base map.

3 Results and discussion

The proposed pipeline not only demonstrates strong robustness and adaptability across varied field layouts owing to its modular spatial analysis approach, but also can be inherently generalized as it relies on point cloud abstraction and graph-based spatial reasoning, unlike crop-specific heuristics. This system can also utilize MST clustering to extract local plant sequences and a global alignment strategy based on unit vector averaging, to reliably identify row and column structures in any crop with a grid-like planting pattern.

The training dataset for the pipeline was obtained from multiple sugarcane farms in Western Uttar Pradesh, during the emergence phase of saplings (30–90 days after planting). The automated detection and gap-mapping workflow enabled rapid identification of bald spots across the surveyed fields, with field-scale germination maps generated within 30 minutes of drone flight processing.

Figure 6 depicts a representation of the output generated by the pipeline. While black dots represent one missing plant, indicating regions not requiring

much intervention, red lines indicate major bald spots by highlighting series of consecutive missing plants (more than two plants), which might require more attention. This enables the identification of regions of high and low germination within the field, allowing for field management backed with practical insights.

This system aims to facilitate timely transplantation interventions in underperforming zones by providing georeferenced maps of missing plants, promoting stand uniformity in corrected plots. In a yield assessment, substantial increase in average yield per acre is expected in fields where transplantation would be guided by the system's recommendations, in comparison to plots without early gap correction.

Moreover, the ability to integrate the output into existing GIS tools allowed farm managers and sugar mills to coordinate harvesting and input supply logistics more efficiently. These findings highlight not only the agronomic value of the approach but also its scalability and economic viability for wide-scale adoption in commercial sugarcane production.

4 Conclusion

The study presented here is a robust and scalable deep learning based computer vision pipeline for automating early-stage sugarcane germination analysis using UAV imagery, YOLOv8 object detection, and spatial point cloud processing. This was done by abstracting dense image data into geometric point clouds and applying graph-based alignment via MST, the system effectively identifies planting rows based upon a moving line identification, detects missing plants, and generates geospatial maps of bald spots. These maps enable timely, site-specific transplantation interventions that improve crop stand uniformity and yield potential. The method is not crop-specific and can be adapted to any row crop with a defined planting geometry, provided inter-row and intra-row distances that follow the grid-like pattern. The Pipeline's modular architecture and lightweight computation conversions also make it suitable for deployment in edge computing or low-resource environments (results illustrated in Table 1).

Overall, this research aims to contribute a practical, interpretable, and high-impact tool that can advance agronomic activities in precision agriculture. Leveraging drone-based remote sensing, machine learning, and geospatial analytics to make more data-driven intelligent decision making at both farm and industry levels.

However, the study has some limitations. The AI model trained for germinated plant detection is not yet fully optimized and requires a larger and more diverse dataset to improve generalization. Agricultural models usually achieve high reliability only when trained on larger spatio-temporal data. To ensure robustness, the pipeline should be validated across at least three to four crop cycles (i.e., spanning 3–4 years on sugarcane) to account for seasonal variability and spatial changes. Future work will focus on testing and robustness of the system to other crops with similar grid-like planting patterns, such as maize, to further evaluate its potential for cross-crop applicability.

5 Acknowledgments

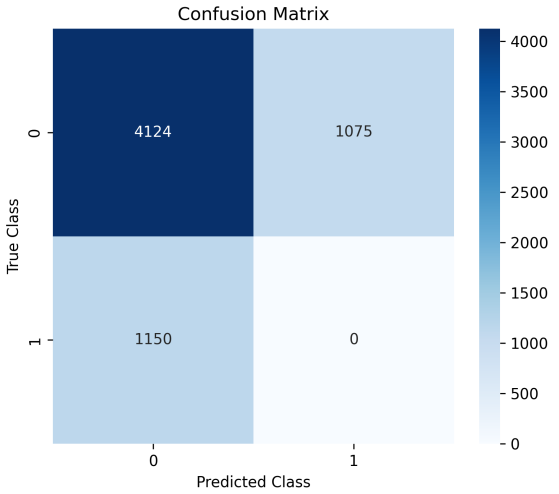
We sincerely thank CNH Industrial for their invaluable support in providing resources and assistance essential to this research. This research would not have been possible without their generous collaboration.

References

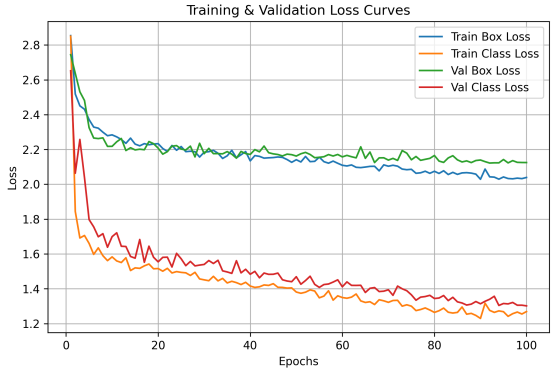
1. Karan Singh, Rajiv Ranjan, Sushil Ghildiyal, Shashank Tamaskar, and Neeraj Goel. 3d-ctm: Unsupervised crop type mapping based on 3-d convolutional autoencoder and satellite image time series. *IEEE Geoscience and Remote Sensing Letters*, 21:1–5, 2024.
2. Rajiv Ranjan, Ying-Jung Chen, Shashank Tamaskar, and Anupam Sobti. Stubble (crop residue) burning detection through satellite images using geospatial foundation model: A case study in punjab, india. In *NeurIPS 2024 Workshop on Tackling Climate Change with Machine Learning*, 2024.
3. Ernst Artschwager and EW Brandes. Sugarcane (saccharum officinarum l.). 1958.
4. India emerges as the world's largest producer and consumer of sugar and world's 2nd largest exporter of sugar. `https://www.pib.gov.in/PressReleseDetailm.aspx?PRID=1865320`, 2023. Accessed: 2025-07-15.
5. Rajiv Ranjan and Shashank Tamaskar. Prediction of sugarcane sucrose content and optimal harvest date using multi-spectral time series image processing of satellite data. In *IGARSS 2024 - 2024 IEEE International Geoscience and Remote Sensing Symposium*, pages 4239–4244, 2024.
6. S Solomon and M Swapna. Indian sugar industry: towards self-reliance for sustainability. *Sugar Tech*, 24(3):630–650, 2022.
7. SM Nalawade, AK Mehta, and AK Sharma. Sugarcane planting techniques: a review. In *Contemporary research in India: National Seminar Recent Trends in Plant Sciences and Agricultural Research (PSAR-2018)*, pages 98–104, 2018.
8. Shiv Pal Singh, Pratap Singh, and AK Tiwari. Factors associated with sugarcane germination. 2019.
9. MA Smit. Characterising the factors that affect germination and emergence in sugarcane. 2010.
10. Kusum Yadav, TK Shrivastava, Pushpa Singh, RK Singh, et al. Navigating sugarcane's growth matrix for yield maximization through ethrel and ga3: Beyond traditions. *Farming & Management*, 9(2):77–91, 2024.
11. Fazlur Rahman and Nida Bee. Trends and pattern of sugarcane production in shahjahanpur district, uttar pradesh: A geographical analysis. *Economic Affairs*, 64(3):537–545, 2019.
12. JV Arun and A Premkumar. Sugarcane growth in india: Problems and prospects: Sugarcane growth in india: Problems and prospects. *SAARC Journal of agriculture*, 20(2):133–144, 2022.
13. Rajiv Ranjan, Tejasvi Birdh, Nandan Mandal, Dinesh Kumar, and Shashank Tamaskar. Evaluating sugarcane yield variability with uav-derived cane height under different water and nitrogen conditions. In Shivakumara Palaiahnakote, Stephanie Schuckers, Jean-Marc Ogier, Prabir Bhattacharya, Umapada Pal, and Saumik Bhattacharya, editors, *Pattern Recognition. ICPR 2024 International Workshops and Challenges*, pages 395–407, Cham, 2025. Springer Nature Switzerland.

14. Rajiv Ranjan, Anit Upadhyaya, Dinesh Kumar, and Shashank Tamaskar. Yield forecasting of sugarcane using machine learning and uav-derived canopy height. In *2024 IEEE India Geoscience and Remote Sensing Symposium (InGARSS)*, pages 1–4, 2024.
15. Sambal Shikhar, Rajiv Ranjan, Aman Sa, Anshika Srivastava, Yash Srivastava, Dinesh Kumar, Shashank Tamaskar, and Anupam Sobti. Evaluation of computer vision pipeline for farm-level analytics: A case study in sugarcane. In *Proceedings of the 7th ACM SIGCAS/SIGCHI Conference on Computing and Sustainable Societies*, COMPASS '24, pages 238–247, New York, NY, USA, 2024. Association for Computing Machinery.
16. Mupparaju Sohan, Thotakura Sai Ram, and Ch Venkata Rami Reddy. A review on yolov8 and its advancements. In *International Conference on Data Intelligence and Cognitive Informatics*, pages 529–545. Springer, 2024.
17. Gary Bradski and Adrian Kaehler. *Learning OpenCV: Computer vision with the OpenCV library.* " O'Reilly Media, Inc.", 2008.
18. Sean Gillies et al. Rasterio: geospatial raster i/o for Python programmers, 2013–.
19. Seth Pettie and Vijaya Ramachandran. An optimal minimum spanning tree algorithm. *Journal of the ACM (JACM)*, 49(1):16–34, 2002.
20. G. R. Charankumar, B. P. Dhyani, . Vivek, U. P. Shahi, Satendra Kumar, and S. P. Singh. Soil fertility status under soils of sugarcane-ratoon-wheat cropping system of meerut district of uttar pradesh, india. *International Journal of Plant; Soil Science*, 34(23):995–1001, Nov. 2022.
21. S. Dhanda, A. Yadav, D. B. Yadav, and B. S. Chauhan. Emerging issues and potential opportunities in the rice-wheat cropping system of north-western india. *Frontiers in Plant Science*, 13:832683, 2022.
22. Francisco-Javier Mesas-Carrascosa, Jorge Torres-Sánchez, Inmaculada Clavero-Rumbao, Alfonso García-Ferrer, Jose-Manuel Peña, Irene Borra-Serrano, and Francisca López-Granados. Assessing optimal flight parameters for generating accurate multispectral orthomosaicks by uav to support site-specific crop management. *Remote Sensing*, 7(10):12793–12814, 2015.
23. Glenn Jocher, Jing Qiu, and Ayush Chaurasia. Ultralytics yolo, 1 2023.
24. R. C. Prim. Shortest connection networks and some generalizations. *The Bell System Technical Journal*, 36(6):1389–1401, 1957.
25. Joseph B. Kruskal. On the shortest spanning subtree of a graph and the traveling salesman problem. *Proceedings of the American Mathematical Society*, 7(1):48–50, 1956.

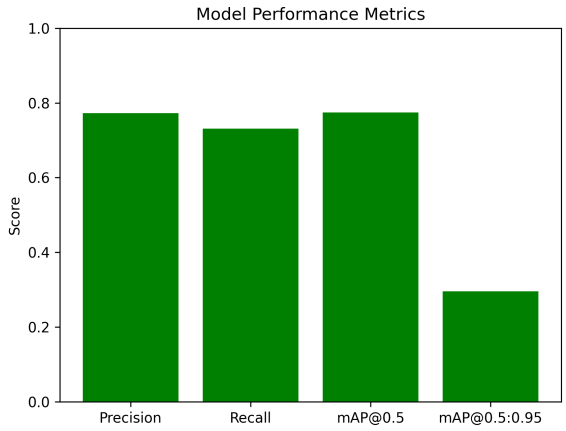
A Model Results



(a) Confusion Matrix



(b) Training vs Validation Loss



(c) Performance Metrics

Fig. 7: Model performance visualizations: (a) Confusion Matrix, (b) Training vs Validation Loss, and (c) Performance Metrics.

Machine	FPS	Avg_time (s)
Intel i5-10500	16.10	0.0621
GTX 1660 SUPER	69.82	0.0143
Raspberry Pi 4 (4GB)	0.94	1.0675
Raspberry Pi 5 (8GB)	2.09	0.7212
Intel Xeon W5	19.63	0.0510

Table 1: YOLOv8 inference performance across different hardware platforms, illustrating the model's scalability from high-performance GPUs to low-power edge devices.